WAAS Signal Deformation Monitor Performance: Beyond the ICAO Threat Model

R. Eric Phelts, *Stanford University*

Karl Shallberg, *Zeta Associates Incorporated*

Todd Walter, Per Enge, *Stanford University*

ABSTRACT

Over nearly 20 years, signal deformation monitoring implementations and research have advanced significantly. Both nominal and anomalous deformations have since been measured on numerous SVs, and sophisticated SBAS and GBAS monitoring algorithms have been exposed to them in real-time. Because of this, the accepted way of modeling signal deformation anomalies—i.e., the ICAO 2nd-Order Step model (with Dead Zones)—has itself come under greater scrutiny. Its continued ability to ensure that existing integrity monitors (previously designed using only that model) can protect against real-world signal deformation threats has yet to be re-assessed. In addition, little has been done to analyze monitor performance against threats outside the original threat model parameter limits.

This paper proposes to assess the current WAAS signal quality monitor algorithm performance against several different kinds of deformation threats. First, it describes three alternative threat model—each extensions of the standard ICAO model, and each designed to more-accurately model past, real-world faults and nominal signal distortions. These alternate threat models include an extended range of standard 2nd-order step parameters, an amplitude-modulated 2nd-order model, and a single-reflection (multipath) model. The WAAS signal quality monitor is validated against each of these. It is shown that the existing WAAS monitor implementation is very capable of detecting many signal deformation threats not previously captured by the standard threat model, despite not having been specifically designed to mitigate them.

BACKGROUND

The first documented signal deformation anomaly was discovered on SV 19 in 1993. Since that time the threat of anomalous signal deformations has existed for users of high-integrity differential GNSS navigation systems [1]. In particular, developers of high-integrity systems like SBAS and GBAS analyzed that event and proposed a class of anomalous distortions that, without monitoring and detection, could pose a hazard to aviation users. Subsequently, a specific threat model that encompassed that thinking was introduced and later adopted as the standard by the International Civil Aviation Organization (ICAO) ICAO and written into the official ICAO "Standards and Recommended Practices" in 2000. [2]

The ICAO signal deformation threat model identified two specific classes of anomalous deformations—digital and analog—to capture the general characteristics of distortions observed on the GPS SV-19 anomaly. It is based on a 2nd-order system model and limited to just three parameters—two for analog/oscillatory effects and one for digital (lead/lag) code distortions [3] [4]. This limited number of parameters provided for simplicity, general flexibility and tractability. This model was designed to be a representative worst-case for signal deformations rather than to model known, specific waveforms. It did not aim to accurately model nominal code distortions. As a result, it does not approximate nominal or near-nominal signals particularly well..

The ICAO fault model was conceived, developed and ultimately adopted by as a standard for modeling this threat before detailed measurements of the signals were readily available or relatively easily obtained. Instead, it was based off of qualitative assessments of a relatively limited amount of chip shape data obtained during the SV-19 incident—the largest GPS signal

deformation event on record—and also differential errors in vertical position recorded by Trimble when the fault was present [5].

The need for a direct relationship to receiver tracking errors led to a model primarily focused on correlation peak distortions. The distortion threats could account for the chip shape-based observations and also ones that create a range of "correlation-peak pathologies"—oscillations, false-peaks, and dead zones—which can lead to large differential range errors for aviation user receivers.

Since the adoption of the ICAO model, real-time signal deformation monitors for GBAS and SBAS have been in operation. The WAAS monitor in particular has provided continuous, real-time monitoring of the GPS C/A code signals for many years [6]. In addition, taking high-resolution measurements of GNSS signals has become more routine [7] [8] [9]. Indeed a number of actual signal deformation faults have been observed and measured using some of the aforementioned techniques as well. Also, there is burgeoning interest in the development of new threat models for GNSS signals on emerging constellations (e.g., Galileo) in the near future [10]. It is likely that all of the more recent developments and observations will inform signal deformation threat models for high-integrity users of these systems.

For all of the aforementioned reasons, questions about the adequacy of the threat model may re-emerge. As a result, a reasonable reassessment of the WAAS monitor against alternative, more-considered threat models can serve to re-assure the aviation integrity community that this monitor can and does continue protect users against credible past and present signal deformation threats.

ALTERNATIVE THREAT MODELS

In the ICAO signal deformation threat model, analog code distortion is modeled using a "2nd-order step" (2OS) filter. (The equations for both analog and digital distortions are provided in Appendix A.) The two parameters of the 2OS model equations—damped oscillation frequency (f_d) and the damping parameters (σ) cannot fully capture some of the behaviors of actual signals. The amplitude is coupled to these two parameters and cannot be independently specified [11]. In addition, the parameter limits specified in the fault model limit the parameter ranges. As a result a large disparity can exist between where nominal deformations end and the fault model begins. The accepted parameter limits for the ICAO threat model are provided in Table 1.

Table 1. Parameter limits for the ICAO 2nd-Order Step Threat Model (with Dead Zones)

	Fault Mode		
Parameter	**(A) Digital-only**	**(B) Analog-Only**	**(C) Analog+Digital**
f_d (MHz)	n/a	4 to 17	7.3 to 13
σ (MNepers/s)	n/a	0.8 to 8.8	0.8 to 8.8
Δ (ns)	-120 to 120	0	-120 to 120

The parameter limits were defined early-on based on their effects on the correlation peak and perceived likelihood of occurrence of each particular fault mode. These limits were also further constrained by the expected performance of receivers and capabilities of monitoring algorithms at the time. The result was a reasonable (albeit somewhat non-intuitive) set of threat constraints. Still, historically, these have proven to create quite challenging deformations for both SBAS and GBAS monitors to provably and reliably mitigate. As a result, extending parameter ranges has seldom been entertained. However, as more data about the measured GNSS signal shapes has become available—both for nominal and faulted signals—interest in providing closer approximations to these observed chip-shapes have arisen.

Figure 1 plots measured, high-resolution traces of the actual nominal transmitted C/A codes of the GPS SVs [7]. (The median of these signals is also plotted as reference.) A single 2nd-order step response with parameters within the specified limits of the full ICAO model is shown for comparison. The frequency, (f_d = 17 MHz) is approximately matched to the observed oscillations on the nominal signals and the damping is maximized (σ=8.8 MNepers/s). At these parameter values, the peak overshoot is far too high and the rise time far too short to approximate nominal signal behavior. Reducing the frequency would bring the rise time more in-line but at the expense of putting the oscillations out-of-phase with the real signals. Peak overshoot generally decreases with increasing frequency, and higher damping could decrease overshoot further, but f_d = 17 MHz and σ=8.8 MNepers/s are already the maximum values the ICAO model parameter limits permit.

Two relatively straightforward modifications to the standard model could be made to potentially fill the gap between the chip responses of the nominal signals and the analog fault model. First, the parameter limits on f_d and σ could be extended until the signals better represent the observations of nominal. Second, a fourth parameter could be added to permit scaling the amplitude independent of the other two. A simple method of doing this is to introduce a parameter that linearly balances the weight to apply to the distortion transfer function relative to an ideal code chip as in the equation below.

$$\tilde{H}_d(s) = a + (1-a)H_d(s), \qquad (1)$$

where $H_d(s)$ is the original transfer function representing the 2nd-order filter of the analog distortions (as described in Equation A-6) and a is the amplitude-weighting factor. In the above equation, a=1 corresponds to zero distortion, or an ideal chip; a=0 corresponds to one distorted by the full weight of the second-order filter.

Figure 2 shows the result of both extending the standard parameter limits on σ. Note that even when σ extends to 25 MNepers/s or 70 MNepers/s and the step responses approach that of the nominal signals in peak overshoot amplitude, their transient response criteria are still coupled. Peak times and rise times still remain too short and vary significantly with σ. Settling time is also affected.

In contrast, applying the amplitude modulation of Eq. 1 can allow the 2OS filter model to more closely match all these nominal transient response criteria. Note, that the discontinuity at the onset of the response is an artifact of this simple model, which scales with an ideal, infinite bandwidth chip. This artifact does not appear after applying bandlimiting from the (monitor or user) receiver filter models—a fundamental part of analyzing the errors associated with all of these modeled distortions.

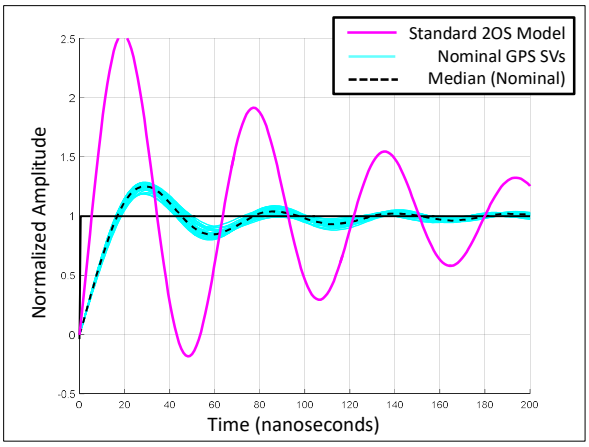

Figure 1. Comparison of a single 2nd-Order Step waveform from the ICAO model to actual nominally distorted GPS C/A code signals.

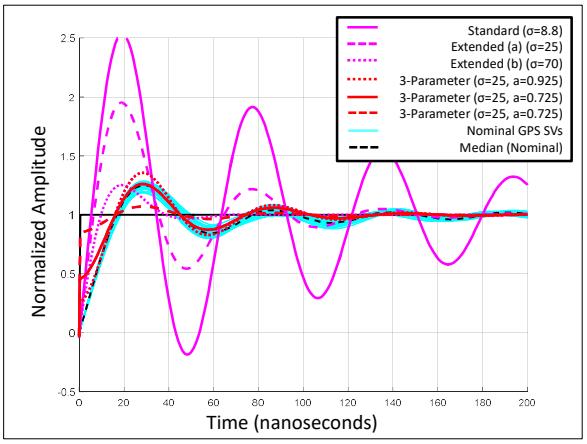

Figure 2. Comparison of three 2nd-Order Step waveforms (with f_d = 17MHz and σ=8.8, 25, and 70MNepers/s) and three amplitude-scaled 2nd-Order Step waveforms (with f_d = 17MHz; σ=25, and a=0.925, 0.725, and 0.625) to nominally distorted GPS signals.

The additional model flexibility afforded by the amplitude modulating parameter seems particularly attractive when attempting to model the more subtle types of distortions that are already known to have occurred [12]. For example, the perturbations that occurred on the chip shape of SVN-54 (PRN-18) appear nearly nominal (See Figure 3). The peak overshoot was primarily affected but also the settling time of the oscillations along the chip seems to have been slightly increased. This distortion could not be reliably captured by the standard ICAO 2OS or even an extended 2OS model. The amplitude-modulated

2OS, however, can approximate this distortion with fd=17 MHz, $8.5 \le \sigma \le 9.0$, and $9.0 \le a \le 9.5$ (Δ is not a relevant parameter here).

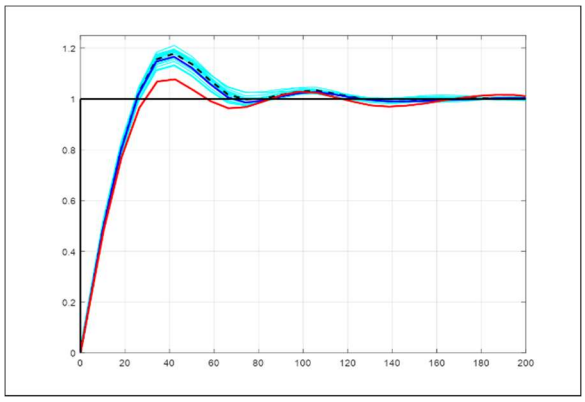

Figure 3. L1 C/A chip shape of SVN-54 (PRN-18) in 2009, as measured by an 18 MHz NovAtel receiver.

An additional type of distortion threat altogether followed in the wake of the launch of SVN-49 in 2009. Multipath on the L1 C/A code signal led to the various levels of chip shapes distortion shown in Figure 3 [13]. (An estimate of the potential effects of this error on WAAS users is given in Appendix B.) This, too, is not well characterized by the two-parameter 2OS filter model.

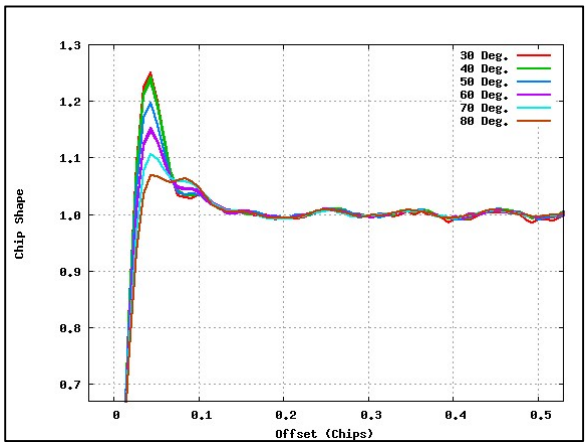

Figure 3. L1 C/A chip shape measured for specific elevation angles for SVN-49 (PRN-01) as measured by an 18 MHz NovAtel receiver.

While this kind of chip shape variation could be approximated by the amplitude-modulated 2OS, the fault itself suggests that a simple signal-reflection model (with a reflected signal scale parameter A and delay offset, d) is a better alternative model against which to test against the WAAS signal deformation monitor. The equation for this threat model— (single) reflection corrupted C/A code $c(t)$ is given below.

$$\begin{aligned} c(t) &= c_{ideal}(t) + A \cdot c_{ideal}(t) \\ &= c_{ideal}(t) + A \cdot c_{ideal}(t-d) \end{aligned} \qquad \text{Eq. 2}$$

The parameter ranges of the reflected code $c_{MP}(t)$= $A \cdot c_{ideal}(t-d)$ are provided in Table 4.

In subsequent sections, the following signal deformation threat models were analyzed to determine the effectiveness of the WAAS signal deformation monitor at mitigating them.

- Standard ICAO Threat Model (Baseline)
- Extended 2nd-order step Model with dead zones
- Amplitude-modulated 2nd-order step Model, with dead zones
- A (single) Signal-Reflection (Multipath) threat model

The parameter limits analyzed for all these models are provided in Tables 1, 2, 3, and 4.

Table 2. Parameter limits for the Extended 2nd-Order Step Threat Model

Parameter	**Analog-Only**
f_d (MHz)	2 to 20
σ (MNepers/s)	0.8 to 25
Δ (ns)	0

Table 3. Parameter limits for the Amplitude-modulated 2nd-Order Step Threat Model (with Dead Zones)

Parameter	**Analog-Only**	**Analog+Digital**
f_d (MHz)	2 to 20	2 to 20
σ (MNepers/s)	0.8 to 25	0.8 to 25
a	0 to 1	0 to 1
Δ (ns)	-120 to 120	-120 to 120

Table 4. Parameter limits for the Single-Reflection (Multipath) Threat Model

Parameter	Range
A	-0.99 to 0.99
d (m)	0 to 100

ANALYSIS METHODOLOGY

For this analysis, only steady-state faults were analyzed. In other words, the faults were assumed to have either 1) occurred on an SV that rises with the fault present or 2) occurs while the WAAS C/A code-based differential correction is active and valid. The latter doesn't not always hold in general, and, in those cases, an additional monitor may be used to help mitigate the threat [14]. In addition, there is no detailed error limit-dependence (i.e., UDRE) of the monitor analyzed here. The UDREs are assumed to be at their smallest value, and the monitor at its maximum sensitivity. This avails the best case scenario for observations (i.e., most averaging) of the faulted signal on the ground, but also bears the most stringent bias requirement. In short, this analysis only answers the question of whether or not these deformations are detectable by the existing WAAS signal deformation monitor. The time-to-alert requirement and other additional operational considerations were not explicitly analyzed here.

The ground monitor/reference model corresponds to a Novatel G-III receiver with a receiver-specific, 24 MHz filter characterization. Narrow-correlator, early-minus-late (EML) tracking at 0.1-chip spacing was used. EML tracking was also assumed for the WAAS user receivers; their filters were as described in [15]. For each threat in the discretized models, range errors and the corresponding threshold-normalized monitor detection metrics were computed. The error-limit analysis described in [16] was applied for each of the threat models to determine whether all the threats can be mitigated and/or if a subset of them remains undetectable and harmful.

The results are discussed in the next section. Deformations that are both hazardous and undetectable would exceed the error limit indicated by the red dashed bounding curve in each of Figures 4, 5, 6, 11, and 14. All others can be considered either detectable by the monitor (i.e., threshold-normalized monitor metric exceeds unity) or otherwise not harmful to users.

RESULTS

Case 0: ICAO 2nd-Order Threat Model (with Dead zones)

The baseline result for mitigation of the standard ICAO threat model is shown in Figure 4. None of the threats come close to exceeding the red-dashed error limit curve in this case. Although some threats remain below the monitor threshold (T=1), their errors are quite small. For reference, also plotted is the WAAS monitor detection/user error region corresponding to nominal GPS C/A code deformations. These nominal deformation biases (and errors) exist for the WAAS monitor and users at all times.

As expected, there is very little overlap between the points in the threat model and the nominal deformations. However, it should be noted that the separation between the two regimes is much less pronounced than might be expected. This is because, due to limited samples of the correlation peak, many parameter combinations can create distortions that appear nearly nominal to the monitor and to the user receivers—i.e., they create minimal distortion and small range errors as well.

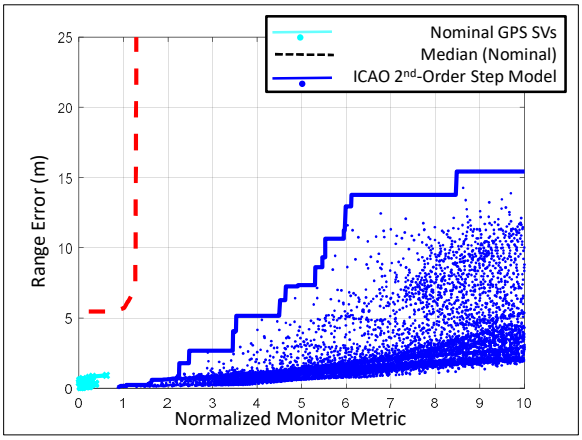

Figure 4. Baseline threat mitigation case: Error vs monitor detection for the ICAO 2OS Threat Model (with Dead Zones).

Case 1: Extended 2nd-Order Threat Model (with Dead zones)

The results for mitigation of the extended 2nd-Order Step threat model is shown in Figure 5. (Note that only the threats what were not included in the original baseline case are plotted here.) Again, no threats come close to exceeding the error limit bound. In fact, this case arguably has as much (or more) performance margin than did the baseline ICAO model (Case 0). Mitigation of these extended threats is somewhat intuitive since (as previously discussed) the transient response criteria for this case seldom approach those of nominal—particularly for the ranges provided in Table 3. Many of these threats are relatively easily detected by the WAAS monitor.

As anticipated, however, there is more overlap here between the model and the nominal deformation data. The model deformation chip shapes (with large damping parameters) do more-closely resemble the measured nominal waveforms. (Refer to Figure 2.) Still, the errors from these extended ICAO threats remain quite small.

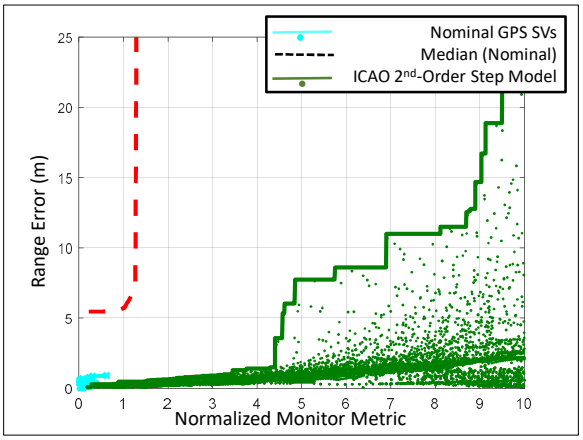

Figure 5. Threat mitigation results for Case 1: Error vs monitor detection for the expanded 2OS Threat Model (with Dead Zones).

Case 2: Amplitude-modulated 2nd-Order Threat Model (with Dead zones)

Error vs. monitor metric results of the amplitude-modulated 2nd-Order Step threat model are shown in Figure 6. Although many of the range errors are significantly larger for this mode (and could potentially pose more of an issue for meeting a time-to-alert requirement), these are still easily mitigated by the monitor in steady-state.

Below the threshold, (T=1), the errors provide even more overlap with the measured nominal data. Indeed the monitor metric goes to nearly zero detectability for some threats. The range errors of the threats approximate those of the nominal data at normalized metric values of approximately 0.5.

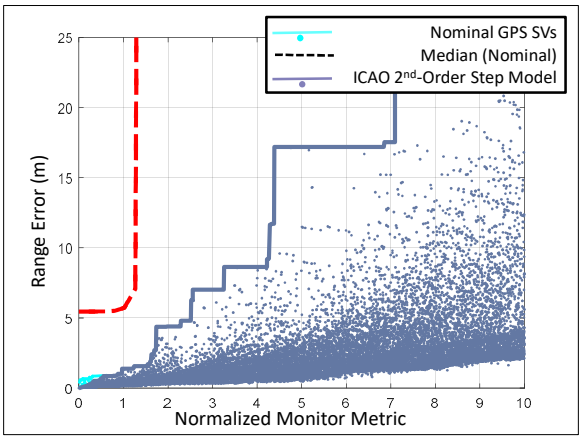

Figure 6. Threat mitigation results for Case 2: Error vs monitor detection for the Amplitude-modulated 2OS Threat Model (with Dead Zones).

Case 3: Single-Reflection Threat Model

The results for the single-reflection threat model are shown in Figure 11. (Note that no digital distortion parameter Δ or dead zone modeling is included in this model.) Notably, a small number of threats do exceed the error bound. The fraction of the threat model that exceeds this limit is quite small (<2%) as is the amount by which they exceed it. Nevertheless, a closer look should be taken at these threats to determine how harmful they are and how they might be mitigated.

Figure 12 shows the parameters corresponding to the undetected threats. They occur for reflections of fairly small amplitude (i.e., akin to those estimated for the SVN-49 anomaly), however the relative delays of these undetected reflections are quite large. In fact, it is implausible to have such large relative delays occur on a satellite signal caused purely by the satellite itself.

Figure 12 plots range error contours for the user receivers that would experience these (hazardous,

undetectable) threats. Predictably, receivers with wide correlator spacings experience far larger errors from these multipath reflections than do those with narrow correlator tracking; the differential errors grows as the correlator spacing increases. Given that the WAAS reference receiver has a correlator spacing of just 0.1-chip (EML), high-quality differential corrections under such conditions are predictably poor for receivers with very wide spacings when subjected to large-delay multipath.

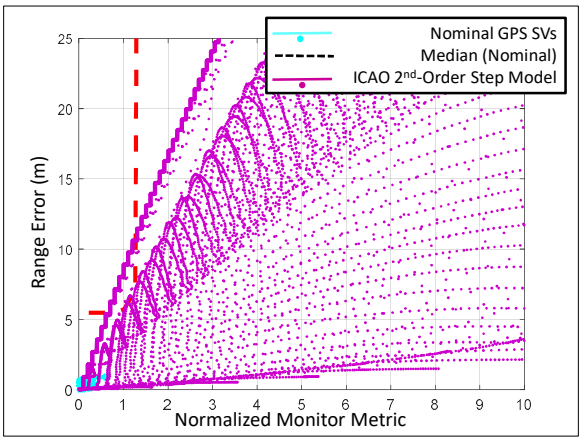

Figure 11. Threat mitigation results for Case 3: Error vs monitor detection for the expanded Single Reflection Threat Model.

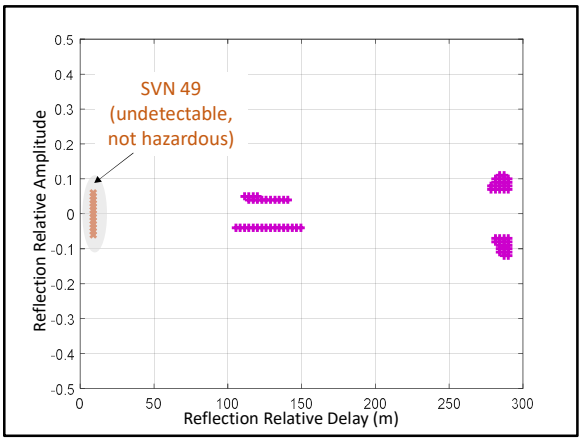

Figure 12. Undetectable threats from Case 3. (SVN 49 approximate parameters shown for reference.)

Figure 13 bears this out. It plots the differential error contours for the undetectable reflection threats. Note that all the harmful errors (i.e., those exceeding the ~5.5m error bound of Figure 11) occur for the narrow bandwidth, wide correlator user receiver configurations. While these configurations are technically part of the Minimum Operational Performance Standard (MOPS DO-229D), no actual receiver manufacturers have equipment there. Current (and future) aviation receivers have always favored narrow correlator, wide-bandwidth designs for the same reasons the ground monitors (and others) do—multipath rejection.

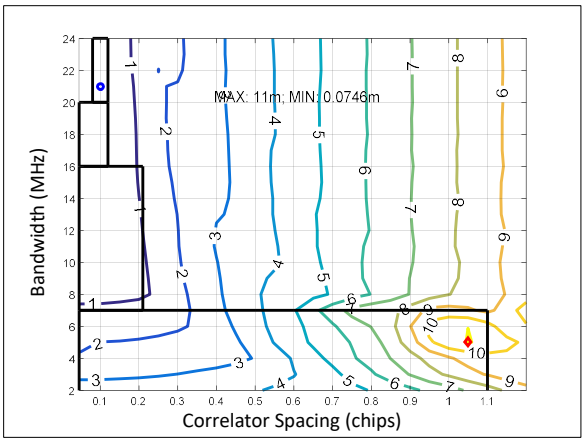

Figure 13. Differential range error contours for undetectable threats from Case 3. (WAAS Reference: 24 MHz, 0.1 chip spacing) MOPS allowed regions are indicated by black borders.

Since this design region is not in use (and not envisioned for future use), if these particular single-reflection threat parameters were a part of an accepted, official threat model that had to be mitigated for safety certification (and if no more monitor re-design were possible), a likely recommendation would simply be to exempt this region from the analysis. Efforts to limit the MOPS user receiver design space in this way (and/or to restrict range of the threat model relative delay parameter itself) would likely go unopposed. Future WAAS receivers propose to restrict this design space even more substantially. [16]

Figure 14 below compares the range error vs. monitor metric bounding curves for each of the four threat model cases in addition to the nominal data. Note that they progressively model the nominal data more accurately. The most pessimistic is the single-reflection model, however, as previously discussed, errors above ~1-meter correspond to user receivers that are not implemented.

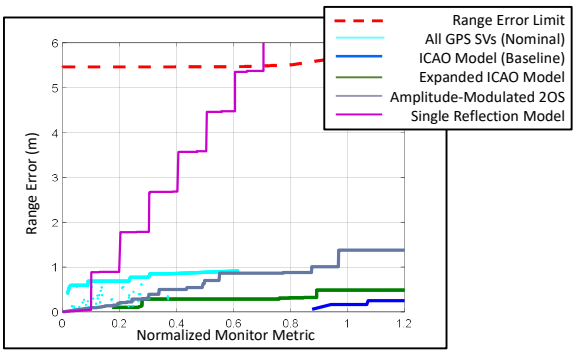

Figure 14. Zoomed plot of Range Error vs. Monitor Metric Bounding curved for all 4 threat model cases and nominal (measured) threats.

CONCLUSIONS

The current WAAS signal quality monitor algorithm steady-state detection performance was assessed against several additional signal deformation threat models. The models were formulated to leverage insight gained from chip-shape measurements of nominal deformations, observed faults, and the official ICAO 2nd-order step threat model. They included an expanded range of ICAO threat parameters, a 4-parameter, amplitude-modulated 2nd-order step model, and a single-reflector, multipath-based threat model.

Although the WAAS monitor was never specifically designed to detect deformations within these threat models, it is able to mitigate nearly all the threats from each of the models fairly easily. The small percentage that could not be detected (and had unacceptably-large range errors) represented threats from the single-reflection (multipath) model. However, these resulted from 1) relative-delays too large to plausibly be induced by a satellite failure, and 2) receivers which do not represent practical, implemented avionics receiver designs (certified for vertical navigation) due to other performance concerns. In short, closing the gaps between the model and nominal (and observed anomalous threats), generally introduces threats that lead to small errors or ones that are easily mitigated by the monitor.

Constraints on the threat models are often not determined by theory alone. Practical considerations of the expected capabilities and performance of the hardware for signals, satellites, and receivers can act to limit an otherwise-straightforward, analytical models in non-intuitive ways. The analysis presented here may help shed light on the process by which some of those decisions can be made about distortion models as yet to be proposed for other GNSS signals in the future.

REFERENCES

[1] Edgar C, Czopek F, Barker B (2000) *A Co-operative Anomaly Resolution on PRN-19,* Proceedings of the 2000 13th International Technical Meeting of the Satellite Division of the Institute of Navigation, ION GPS-2000. Proceedings of ION GPS 2000, v 2, pp. 2269-271.

[2] "International Standards and Recommended Practices," *Aeronautical Telecommunications*, ICAO, Vol. 1, Annex 10, July 2006.

[3] Enge P.K., Phelts R. E., Mitelman A. M., (1999) *Detecting Anomalous signals from GPS Satellites,* ICAO, GNSS/P, Toulouse, France.

[4] Phelts, R. E. (2001) *Multicorrelator Techniques for Robust Mitigation of Threats to GPS Signal Quality*, Ph.D. Thesis, Stanford University, Stanford, CA.

[5] Mitelman A. M. (2005) *Signal Quality Monitoring For GPS Augmentation Systems,* Ph.D. Thesis, Stanford University, Stanford, CA.

[6] Phelts R.E., Altshuler E, Walter T, Enge P, "Validating Nominal Bias Error Limits Using 4 years of WAAS Signal Quality Monitoring Data", ION Pacific PNT 2015

[7] Wong, G., Phelts, R.E., Walter, T., Enge, P., "Alternative Characterization of Analog Signal Deformation for GNSS-GPS Satellites," *Proceedings of the 2011 International Technical Meeting of The Institute of Navigation*, San Diego, CA, January 2011, pp. 497-507.

[8] Thoelert, S., Enneking, C., Vergara, M., Sgammini, M., Antreich, F., Meurer, M., Brocard, D., Rodriguez, C., "GNSS Nominal Signal Distortions - Estimation, Validation and Impact on Receiver Performance," *Proceedings of the 28th International Technical Meeting of The Satellite Division of the Institute of Navigation (ION GNSS+ 2015)*, Tampa, Florida, September 2015, pp. 1902-1923.

[9] York, Johnathan, Joplin, Andrew, Bratton, Michael, Munton, David, "A Detailed Analysis of

GPS Live-Sky Signals Without a Dish", *NAVIGATION, Journal of The Institute of Navigation*, Vol. 61, No. 4, Winter 2014, pp. 311-322.

[10] Pagot, Jean-Baptiste (2016) *Modeling an Monitoring of new GNSS Signal Distortions in the Context of Civil Aviation,* Ph.D. Thesis, l'Institut Nationale Polytechnique de Toulouse, Toulouse, France.

[11] Phelts, R.E., Walter, T., Enge, P., "Characterizing Nominal Analog Signal Deformation on GNSS Signals," *Proceedings of the 22nd International Technical Meeting of The Satellite Division of the Institute of Navigation (ION GNSS 2009)*, Savannah, GA, September 2009, pp. 1343-1350

[12] Shallberg, Karl W., Ericson, Swen D., Phelts, Eric, Walter, Todd, Kovach, Karl, Altshuler, Eric, "Catalog and Description of GPS and WAAS L1 C/A Signal Deformation Events," *Proceedings of the 2017 International Technical Meeting of The Institute of Navigation*, Monterey, California, January 2017, pp. 508-520.

[13] Ericson S, Shallberg K, Edgar C, "Characterization and Simulation of SVN49 (PRN01) Elevation Dependent Measurement Biases", ITM 2010

[14] Shloss, P., Phelts, R. E., Walter, T., Enge, P., "A Simple Method of Signal Quality Monitoring for WAAS LNAV/VNAV," *Proceedings of the 15th International Technical Meeting of the Satellite Division of the Institute of Navigation*, ION GPS/GNSS-2002, September 2002.

[15] Minimum Operational Performance Standards (MOPS) for WAAS, DO-229D. *RTCA*.

[16] Phelts RE, Wong G, Walter T, Enge P, "Signal Deformation Monitoring for Dual-Frequency WAAS", ITM 2013

APPENDIX A: Mathematical Models of Signals and the ICAO 2nd-order Step Model with Dead Zones

The analysis of this paper assumes the incoming signals have been translated to baseband and are phase locked with zero phase error. To model a BOC(*n,m*) code at a chipping rate of *m**1.023MHz, the following equation may be used

$$c_{n,m}(t) = c_{\mathrm{m}}(t) \cdot \mathrm{s}_{\mathrm{n}}(t) \qquad \text{(A-1)}$$

where $\mathrm{s}_{\mathrm{n}}(t)$ is a square wave of frequency *n**1.023MHz. (For this paper, the GPS PRN-01 was used for $c_{\mathrm{m}}(t)$. And C/A code was assumed such that *n*=0 and *m*=1.) A square wave was then modulated onto it at a frequency of 1.023MHz.

Code distortion may be analyzed by examining the autocorrelation functions. The ideal autocorrelation function ${}_{n,m}R(\tau)$ is given by

$${}_{n,m}R(\tau) = \int_{-\infty}^{\infty} {}_{n,m}H(f)\,{}_{n,m}C(f)\,{}_{n,m}C_R^*(f)e^{j2\pi f}df \qquad \text{(A-2)}$$

where, ${}_{n,m}H(f)$ represents the transfer function of the combined filter that affect the incoming signal $C(f)$. For accurate modeling, ${}_{n,m}H(f)$ should include the filters on the satellite, the antenna and LNA, and inside the receiver. $C_R^*(f)$ is the complex conjugate of the power spectrum of the replica code.

Correlation Peak Distortion models

A digital lead/lag distortion can be modeled as a circular shift of a single code sequence added/subtracted from a standard code sequence. A general equation for modeling lead or lag distortions is given below

$${}_{n,m}c_{\Delta}(t) = \begin{cases} \max\left[\left({}_{n,m}c(t+\Delta) - {}_{n.m}c(t)\right),0\right], & \Delta \le 0 \\ \min\left[\left({}_{n,m}c(t+\Delta) - {}_{n.m}c(t)\right),0\right], & otherwise \end{cases} \qquad \text{(A-3)}$$

$${}_{n,m}c_{d(\Delta)}(t) = {}_{n,m}c(t) + {}_{n,m}c_{\Delta}(t) \qquad \text{(A-4)}$$

It follows that a correlation peak distorted by this failure mode is found from

$${}_{n,m}R_{d(\Delta)}(\tau) = \int_{-\infty}^{\infty} {}_{n,m}H(f)\,{}_{n,m}C_{d(\Delta)}(f)\,{}_{n,m}C_R^*(f)e^{j2\pi f}df \qquad \text{(A-5)}$$

Where ${}_{n,m}C_{d(\Delta)}$ is the frequency domain representation of the digitally-distorted code, ${}_{n,m}c_{d(\Delta)}(t)$.

The transfer function of the 2nd-order filter for representing the analog failure mode is given by

$$H_d(s) = \frac{(\omega_0)^2}{s^2 + 2\zeta\omega_0 s + (\omega_0)^2} \qquad \text{(A-6)}$$

where $\sigma = \zeta\omega_0$ (the product of the damping ratio ζ and the natural frequency ω_0) and is defined as the damping/attenuation factor, σ in MNepers/sec. The damped frequency of oscillation, F_d, is found from

$$F_d = \frac{1}{2\pi}\sqrt{1-\zeta^2} \qquad \text{(A-7)}$$

Using this filter to modify the incoming signal yields the following expression for the deformed correlation peak

$${}_{n,m}R_{d(fd,\sigma)}(\tau) = \int_{-\infty}^{\infty} H_d(f)\,{}_{n.m}H(f)\,{}_{n.m}C(f)\,{}_{n.m}C_R^*(f)e^{j2\pi f}df \qquad \text{(A-8)}$$

where we have substituted $s = \sigma + 2\pi jf$, into $H_d(s)$ to produce $H_d(f)$ as the frequency domain representation of the 2nd-order response filter function.

The equation for the correlation function of a signal affected by both analog and digital failure modes is provided below.

$${}_{n,m}R_{d(fd,\sigma,\Delta)}(\tau) = \int_{-\infty}^{\infty} H_d(f)\,{}_{n,m}H(f)\,{}_{n,m}C_{d(\Delta)}(f)\,{}_{n,m}C_R^*(f)e^{j2\pi f}df \qquad \text{(A-9)}$$

APPENDIX B: SVN49 Tracking Errors for WAAS Users

A data-validated multipath model for the SVN49 L1 C/A code signal was proposed in the paper entitled "Characterization of SVN49 (PRN-1) Elevation Angle Dependent Measurement Biases" by Ericsson, Shallberg, and Edgar and presented at the ITM 2010 Conference. [13] This appendix uses that model to estimate the worst-case errors a WAAS user might experience due to tracking the SVN49 signal.

Analysis

The line-of-sight correlation peak was modeled as $R(\tau)$ coherent tracking with zero phase error was assumed. The reflected peak was formed by adding $R(\tau)$ to two additional peaks modified by relative magnitudes, phases and delays. The relative magnitudes and phases of the two reflections were as defined in columns Table of [13]. The relative delays for each reflection were 31ns and 62ns, respectively. For each elevation angle, the combined peaks were subsequently filtered using the accepted WAAS G-II filter characterization file.

The tracking errors for early-minus-late (EML) receiver configurations with correlator spacing *d* chips are computed using

$$\tau_{EML} = \arg\left[R(\tau - d/2) - R(\tau + d/2)\right] \quad \text{(B-1)}$$

where *d* represents the correlator spacing of the EML delay-lock loop. (The WAAS reference receiver uses an EML correlator spacing of 0.1 chips.)

The tracking errors for double-delta (ΔΔ) user receivers are found by combining two early-minus-late discriminators according to

$$\tau_{\Delta\Delta} = \arg\{2*[R(\tau - d_1/2) - R(\tau + d_1/2)] - [R(\tau - d_2/2) - R(\tau + d_2/2)]\}, \quad d_2 = 2 \cdot d_1 \quad \text{(B-2)}$$

The constraints on user receiver pre-correlation bandwidths and correlator spacings are provided in the MOPS DO-229D. [15] The figures therein are repeated in Figures B-1 and B-2 below. (Group delay variations were also modeled as constrained in the MOPS DO-229D. These details are not described here.)

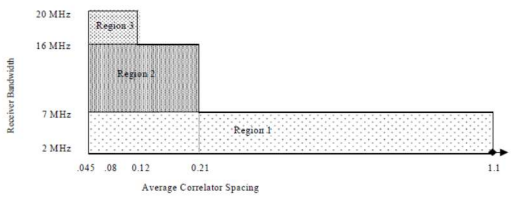

Figure B-1. Early-minus-late receiver design constraint regions. (MOPS DO-229D Figure 2-2A) [15]

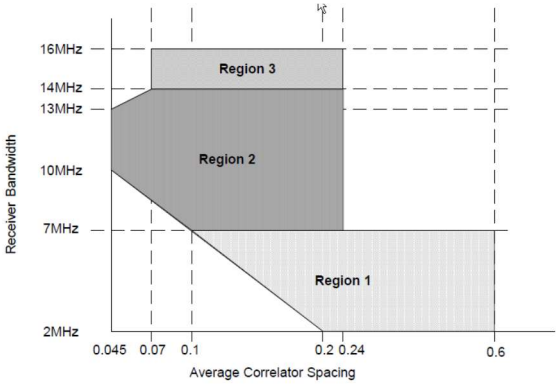

Figure B-2. Double-delta receiver design constraint regions. (MOPS DO-229D Figure 2-2A) [15]

Results

The maximum tracking errors for all allowed EML and ΔΔ user receivers are shown in Figures B-3 and B-4. Figure B-3 plots the maximum error magnitude for allowed users given the reflections as defined by Table 1. Figure B-4 plots the same results for the case where the relative phases of the reflections are modified by +8 degrees. This latter correction was noted in the paper by Ericsson, et al to provide slightly better agreement with the data. (Note that the absolute value is not taken for the errors in this latter case.)

Both figures plot both uncorrected and corrected versions of the errors for each of the two receiver discriminator types. The uncorrected curves assume the WAAS network is able to completely calibrate and remove this bias from its differential corrections. The other two curves reveal biases that would remain when a differential correction is applied. This latter case represents the best a local area differential system—whose elevation angles do not differ from those of the user—could correct SVN-49 biases. WAAS users

probably have errors somewhere in-between these two extremes.

The upper limit of the uncorrected user error is approximately 2 meters; for the differentially-corrected case, the maximum is about 0.7 meters. The case without the 8-degree phase correction case is slightly more pessimistic at large elevation angles. Note that at low elevation angles, the errors are nonzero. This suggests that some small nominal biases may exist due to the presence of these reflections regardless of elevation angle.

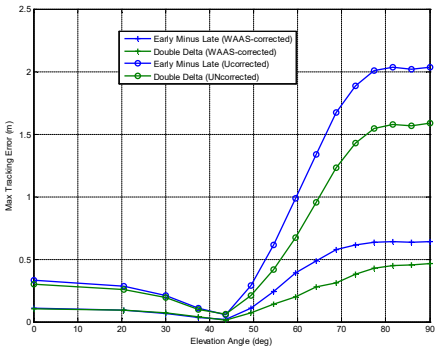

Figure B-3. Maximum User Errors (Magnitudes) for the 2-Reflection Case.

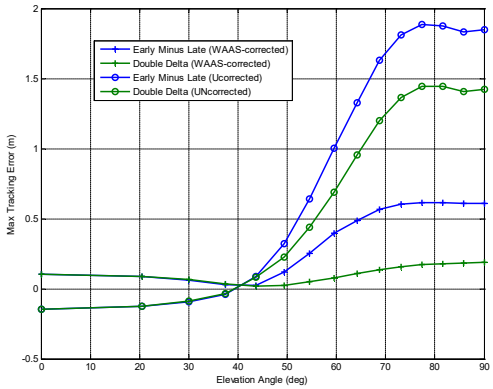

Figure B-4. Maximum User Errors for the 2-Reflection Case – Phase Values Modified by +8 degrees. (No absolute value.)